LAWRENCE
LIVERMORE
NATIONAL
LABORATORY

Vector Finite Element Modeling of the Full-Wave Maxwell Equations to Evaluate Power Loss in Bent Optical Fibers

J. Koning, R. Rieben, G. Rodrigue

December 14, 2004

Disclaimer

Vector Finite Element Modeling of the Full-Wave Maxwell Equations to Evaluate Power Loss in Bent Optical Fibers

J. Koning   R. Rieben   and G. Rodrigue

Abstract

We measure the loss of power incurred by the bending of a single mode step-indexed optical fiber using vector finite element modeling of the full-wave Maxwell equations in the optical regime. We demonstrate fewer grid elements can be used to model light transmission in longer fiber lengths by using high-order basis functions in conjunction with a high order energy conserving time integration method. The power in the core is measured at several points to determine the percentage loss. We also demonstrate the effect of bending on the light polarization.

I. INTRODUCTION

The accurate characterization of signal loss due to wave attenuation is a valuable measure of the reliability of a communication system. This is particularly important in light wave communication systems where wave attenuation limits the performance of the optical fiber as a data transmission channel. Although spectacular success has been achieved in the development of low-loss optical fibers, signal attenuation can still occur from a variety of sources. Intrinsic glass manufacturing inconsistencies can cause wave attenuation through the scattering and absorption of light energy. Attenuation from these sources can range from 0.5 db/km to 1000 db/km and is dependent on the material of the particular optical fiber.

Wave attenuation from external sources are more difficult to characterize as they can arise from many factors. This paper focuses on measuring wave attenuation due to the bending of an optical fiber. Local bending causes wave attenuation by changing the refractive properties of the fiber thereby causing light energy to radiate away from the guiding direction. Power loss from fiber bending is generally estimated using theoretical predictions obtained from an analysis of the equations that result from an asymptotic assumption on the cladding radius, curvature radius or refractive index difference, [1], [2]. Power losses from the transition of the fiber from straight to curve, [3], or at the outer portion of the evanescent field, [4], can be derived in this manner. The disadvantage of these approaches is their reliance on techniques of asymptotic analysis whereby mathematical terms in equations are rendered unimportant because of their dependence on parameters that are assumed to be very small. Power loss measurements from these approaches can only be assumed accurate under extreme conditions.

We demonstrate in this paper how power loss measurements of a bent optical fiber can be effectively calculated by numerically solving the full wave Maxwell equations. Discretization of Maxwell's equations will be provided by the finite element method on hexahedral grids, [5], [6]. This will allow for power loss measurements to be calculated under more realistic curved geometries. High-order Nedelec basis functions are used to provide numerical approximations to the fields, [7], [8]. Then, coarse grids can be used to represent the geometry while still maintaining numerical accuracy and preserving the continuity properties of the fields across material interfaces. High order integrations are used to time evolve the equations so that energy conservation and numerical dispersion errors are kept at a minimum, [9]. We should mention that other power loss computations on bent fibers have been done. However, assumptions are made on the bent fiber so that the dynamics of the light waves can be modeled by a reduced Maxwell equations on an equivalent straight waveguide, [10], [11].

II. MAXWELL'S EQUATIONS

The dynamical behavior of light waves in a lossless region Ω are modeled by the full-wave Maxwell equations

$$
\begin{aligned}
\varepsilon\frac{\partial}{\partial t}\mathbf{E} &= \nabla \times (\mu^{-1}\mathbf{B}) &&\text{in } \Omega \\
\frac{\partial}{\partial t}\mathbf{B} &= -\nabla \times \mathbf{E} &&\text{in } \Omega
\end{aligned}
\tag{1}
$$

We impose the physical restriction that there are no free electric or magnetic charges in the problem domain, yielding the constraints

$$
\begin{aligned}
\nabla \cdot (\varepsilon\mathbf{E}) &= 0 &&\text{in } \Omega \\
\nabla \cdot \mathbf{B} &= 0 &&\text{in } \Omega
\end{aligned}
\tag{2}
$$

Initial-boundary values are given by

$$\begin{aligned}
\hat{\mathbf{n}} \times \mathbf{E} &= \mathbf{E}_{bc} \quad \text{on } \partial\Omega \\
\mathbf{E}(t) &= \mathbf{E}_{ic} \quad \text{at } t = t_0 \\
\mathbf{B}(t) &= \mathbf{B}_{ic} \quad \text{at } t = t_0
\end{aligned} \tag{3}$$

The symbol $\partial\Omega$ is the two dimensional boundary of the domain Ω with an outwardly directed unit normal $\hat{\mathbf{n}}$. The symbols ε and μ are the electric permitivity and magnetic permeability describing the material properties of the region Ω. These parameters are free to be tensor valued, possibly discontinuous functions of space; however, we impose the restriction that they are linear and independent of time.

The variational form of (1) is

$$\int_\Omega \varepsilon \frac{\partial}{\partial t} \mathbf{E} \cdot \mathbf{W} = \int_\Omega \frac{1}{\mu} \mathbf{B} \cdot \nabla \times \mathbf{W} - \oint_{\partial\Omega} \left(\frac{1}{\mu}\mathbf{B} \times \mathbf{W}\right) \cdot \hat{\mathbf{n}} \tag{4}$$

$$\int_\Omega \frac{1}{\mu} \frac{\partial}{\partial t} \mathbf{B} \cdot \mathbf{F} = -\int_\Omega \frac{1}{\mu} \nabla \times \mathbf{E} \cdot \mathbf{F}$$

for all test functions $\mathbf{W}, \mathbf{F}$, such that

$$\begin{aligned}
\mathbf{W} \in H(curl, \Omega) &= \{\mathbf{u}: \ \nabla \times \mathbf{u} \in [L_2(\Omega)]^3\} \tag{5} \\
\mathbf{F} \in H(div, \Omega) &= \{\mathbf{u}: \ \nabla \cdot \mathbf{u} \in L_2(\Omega)\} \tag{6}
\end{aligned}$$

We employ a Galerkin approximation using a finite dimensional vector basis expansion of arbitrary polynomial degree [6]

$$\mathbf{E}(\mathbf{r}, t) \approx \sum_i^{N_W} e_i(t) \mathbf{W}_i(\mathbf{r}), \quad \mathbf{W}_i \in H(curl, \Omega) \tag{7}$$

$$\mathbf{B}(\mathbf{r}, t) \approx \sum_i^{N_F} b_i(t) \mathbf{F}_i(\mathbf{r}), \quad \mathbf{F}_i \in H(div, \Omega) \tag{8}$$

which upon substitution into (4) yields the semi-discrete system of ordinary differential equations

$$\begin{aligned}
M_\varepsilon \frac{\partial}{\partial t} e &= K^T M_\mu b \tag{9} \\
\frac{\partial}{\partial t} b &= -K e
\end{aligned}$$

Here, K is the discrete curl matrix, M_ε, M_μ are the mass matrices associated with basis functions $\{\mathbf{W}_i\}$, $\{\mathbf{F}_i\}$, respectively, and e, b are vectors of the electric and magnetic field degrees of freedom. For a fixed integer p, the finite dimensional spaces

$$\begin{aligned}
\mathbf{W}^p &= span[\mathbf{W}_1, \mathbf{W}_2, \ldots, \mathbf{W}_{N_W}] \subset H(curl, \Omega) \\
\mathbf{F}^p &= span[\mathbf{F}_1, \mathbf{F}_2, \ldots, \mathbf{F}_{N_F}] \subset H(div, \Omega)
\end{aligned}$$

are contained in the polynomial spaces

$$\begin{aligned}
\Pi_W &= Q_{p-1,p,p} \otimes Q_{p,p-1,p} \otimes Q_{p,p,p-1} \\
\Pi_F &= Q_{p,p-1,p-1} \otimes Q_{p-1,p,p-1} \otimes Q_{p-1,p-1,p}
\end{aligned}$$

where $Q_{l,m,n}$ denotes a polynomial in the variables (x, y, z) whose maximum degree is l in x, m in y and n in z. The vector polynomial basis functions $\{\mathbf{W}_i\}$, $\{\mathbf{F}_i\}$ are defined piecewise on the hexahedral elements of a computational grid through a transformation of vector polynomial basis functions defined on a unit reference element $0 \leq x, y, z \leq 1$. Although simply stated, this is a complicated procedure and details of their construction can be found in [6]. For a polynomial basis order p, the approximation of (7) is $p+1$ order accurate in Δh, the characteristic volume of the hexahedral element.

High order and energy conserving time-integration of (9) is given by a generalized symplectic update [9]

$$\begin{bmatrix} e_{n+1} \\ b_{n+1} \end{bmatrix} = \left(\prod_{i=1}^{k} Q_i\right) \begin{bmatrix} e_n \\ b_n \end{bmatrix} \tag{10}$$

where k is the order of the symplectic integration method and the matrices Q_i are of the form

$$Q_i = \begin{bmatrix} I & \beta_i \Delta t \, M_\varepsilon^{-1} K^T M_\mu \\ -\alpha_i \Delta t K & I - \alpha_i \beta_i \Delta t^2 K \, M_\varepsilon^{-1} K^T M_\mu \end{bmatrix} \tag{11}$$

and Δt is the discrete time step. The integration coefficients in (11) are listed in Table I. In this particular mixed finite element method the instantaneous energy is the numerical version of the total energy stored in the electric and magnetic fields. It is computed as

$$\tilde{\mathcal{E}} = e^T M_\varepsilon \, e + b^T M_\mu \, b \tag{12}$$

Order 1	
$\alpha_1 = 1$	$\beta_1 = 1$
Order 2	
$\alpha_1 = 1/2$	$\beta_1 = 0$
$\alpha_2 = 1/2$	$\beta_2 = 1$
Order 3	
$\alpha_1 = 2/3$	$\beta_1 = 7/24$
$\alpha_2 = -2/3$	$\beta_2 = 3/4$
$\alpha_3 = 1$	$\beta_3 = -1/24$

TABLE I

SYMPLECTIC INTEGRATION COEFFICIENTS FOR METHODS OF ORDER 1,2 AND 3

III. NUMERICAL RESULTS

In the following computational experiments, we simulate the propagation of an optical pulse along a $155\mu m$ section of a single mode optical fiber. The core of the fiber has a radius of $5\mu m$ and an index of refraction of 1.471 while the cladding has a radius of $40\mu m$ and an index of refraction of 1.456. With these properties, the fiber is capable of propagating a $\lambda = 1.55\mu m$ optical wave. The ratio of problem domain size to wavelength is therefore $\Omega/\lambda = 100$ making this an "electrically large" problem. The problem is excited with a space and time dependent pulsed voltage source boundary condition applied to the input cap of the fiber representing a TE01 polarized mode. The spatial dependence of the voltage source is derived from Bessel functions of the first and second kind with the appropriate transverse propagation constants to satisfy continuity across the core / cladding interface while the temporal profile is a Gaussian pulsed sine wave containing 20 wavelengths as shown in Figure 1.
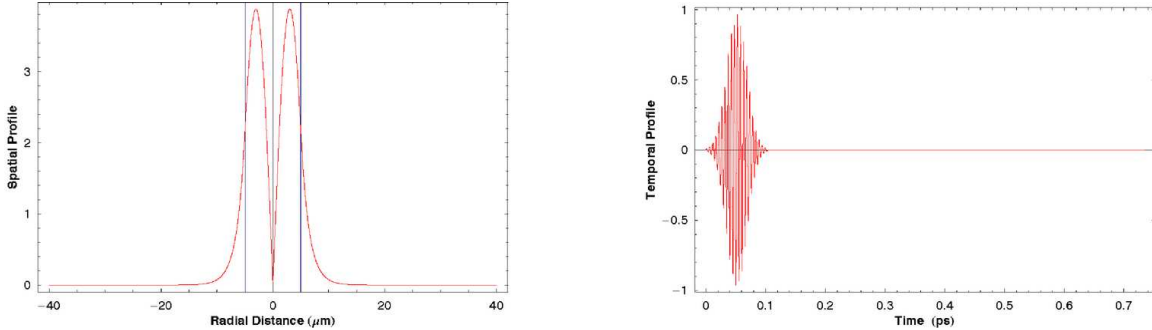

Fig. 1.   Spatial and temporal profile of pulsed voltage used to excite fiber optic simulation

We perform the simulation using a straight fiber as reference and four bent fibers with different bend angles as summarized in Table II. The loss due to curvature of an optical fiber has been studied extensively and it is well well known that fiber waveguides lose power by radiation if their propagation axes are curved. As pointed out in [4], even if the standard radiation loss of the fiber is disregarded, the field changes its shape in the curved guide (known as the bend loss); the field is forced toward the outer wall in a manner resembling a centrifugal force effect. Only for very large bending radius values is it permissible to neglect this effect; for sharply curved guides the field distortion caused by the bend has a considerable influence on the curvature loss. Bending losses in fibers are therefore classified as either macro-scale or micro-scale. It is well known that losses due to macro-scale bends where the bending radius is greater than $10cm$ are essentially negligible [12]. Transmission in a fiber with a bending radius smaller than this is subject to signal loss due to radiation and bend loss [3].

We decompose the domain of the fiber into a mesh of hexahedral elements and two material regions, namely the core and the cladding. Because the problem is electrically large, it will be subject to the cumulative errors of numerical dispersion. To mitigate this effect, we use high order polynomial basis functions of degree $p = 2$ in conjunction with a high order symplectic (energy conserving) integrator of order $k = 3$ which has been shown to excel at reducing the effects of numerical dispersion for electrically large time domain problems [6]. The computational mesh for each of the five simulations consists of $147,200$ hexahedral elements with 4 transverse elements per wavelength, an example of which is shown in Figure 2. Note that 4 transverse elements per wavelength is significantly less than the commonly used heuristic of 10 transverse cells per wavelength for standard low order finite element approximations. Using high order $p = 2$ basis functions on this mesh results in a semi-discrete linear system (9) consisting of $3,562,160$ electric field unknowns and $3,547,072$ magnetic flux density unknowns. This relatively large problem must therefore be solved in a parallel computational environment. The computational statistics

Bend Angle	Bend Radius	Fiber Length
0^0 (*straight*)	∞	155 μm
15^0	592.056 μm	155 μm
30^0	296.028 μm	155 μm
45^0	197.352 μm	155 μm
60^0	148.014 μm	155 μm

TABLE II

BEND ANGLE AND RADIUS FOR VARIOUS FIBER OPTIC MESHES
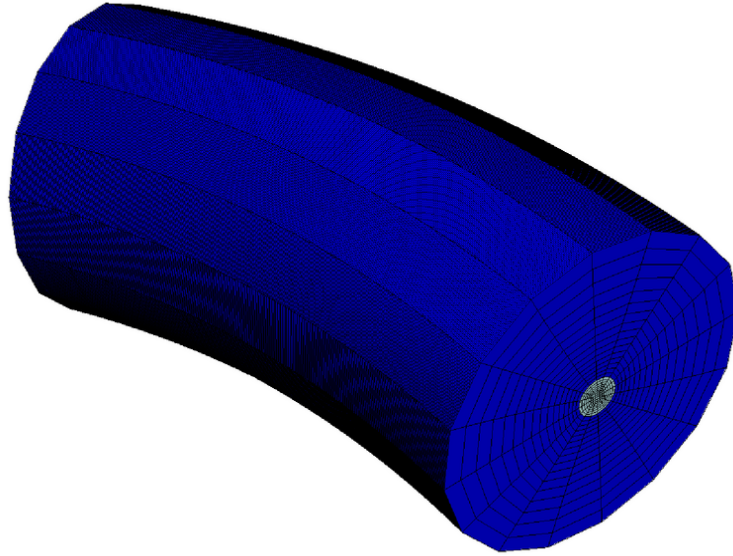
for each of the five simulations are summarized in Table III.

Fig. 2.   Example of the computational fiber mesh

In Figure 3 we plot the normalized energy in the fiber core, computed by (12), as a function of time for each of the five fiber simulations. The energy is normalized to the total energy of the optical pulse. As expected, the energy in the straight fiber is confined in the core for the duration of the simulation and is roughly 86% of the total pulse energy. As the fiber is bent, the energy in the core is lost due to radiation in the cladding as the pulse traverses the bend. This effect becomes more drastic as the bend angle (bend radius) increases (decreases) and as time increases. Note that for the 60 degree bent fiber, the core energy loss at time $t = 0.36ps$ is very close to 100%. In Figure 3 we plot the base 10 log of the electromagnetic field energy, as computed by (12), for the 30 degree bent fiber at four separate snapshots in time. As the pulse traverses the bend, the majority of the energy is radiated into the cladding, and the remaining energy still guided in the core diminishes rapidly as a function of time. It is important to point out that the cladding radius of $40\mu m$ we have used for our simulations is significantly smaller than the typical radius of $120\mu m$ used in commercial grade single mode fibers. This is due to the limits of computational resources.

In Figure 5–Figure 9 we plot the base 10 log of the magnitude of the Poynting field, $\log_{10}(\sqrt{\mathbf{P} \cdot \mathbf{P}})$ where $\mathbf{P} = \mathbf{E} \times \mathbf{B}$, at time $t = 0.36ps$ for each of the five fiber simulations. The Poynting field can be used as a measure of power loss in the fiber core. Note that the majority of the power is confined in the core for the case of the straight fiber while the power loss increases dramatically as the fiber is bent. In Figure 10–Figure 14 we plot a two dimensional "slice" of the electric field vector at time $t = 0.36ps$ for each of the five fiber simulations. Each plot is sliced in a plane that is normal to the tangent curve of the fiber bend. Note that for the straight fiber, the electric field remains circularly polarized as one would expect for a TE01 mode. However, as the bend angle increases and the electric field begins to radiate into the cladding, the orientation of the electric field becomes considerably more complex.

No. Hexahedral Mesh Elements	147,200
No. E-Field Unknowns	3,562,160
No. B-Field Unknowns	3,547,072
No. Parallel CPUs Per Simulation	64
Total Physical Time	0.73333 ps
Discrete Time Step	3.3333e-4 ps
No. Time Steps	2200
No. Linear Solves Per Step	3

TABLE III

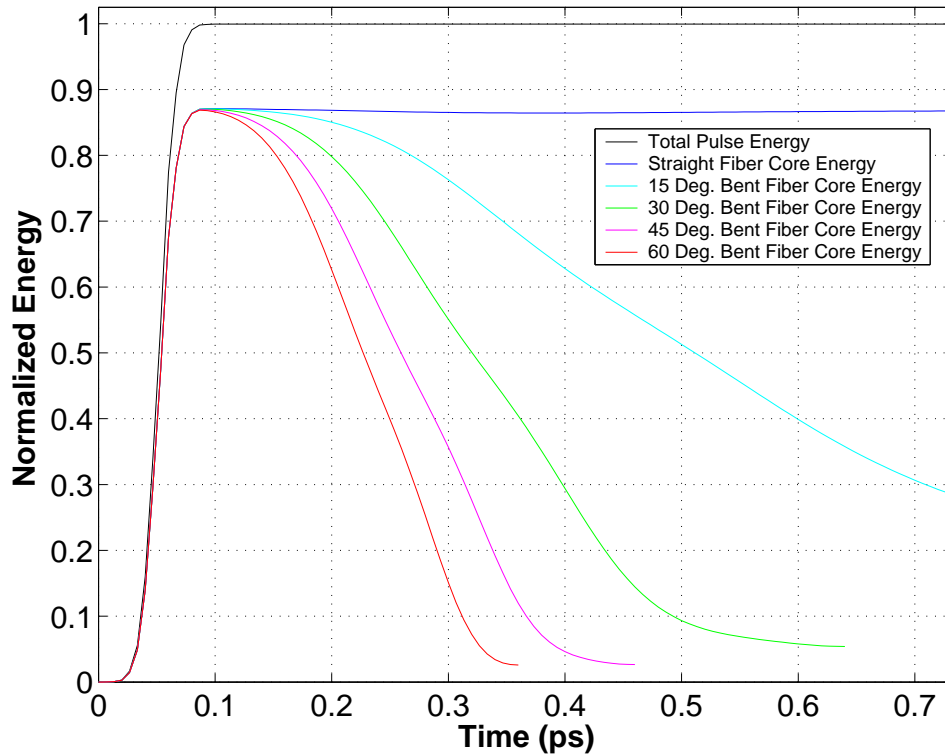SUMMARY OF COMPUTATIONAL STATISTICS FOR FIBER SIMULATIONS

Fig. 3. Normalized core energy as a function of time for each of the five fiber simulations

IV. CONCLUSIONS

Computer modeling of wave propagation in complicated optical communication devices is difficult to perform because of the complex geometries and the highly restrictive time scales. However, the progress of vector finite element modeling coupled with the advances in high speed computing environments has now made it possible to perform these complicated simulations and to make accurate measurements of interest to the optical engineering community. This was demonstrated here by modeling for the first time the classical problem of wave propagation in a bent optical fiber using the full wave Maxwell's equations. Power loss measurements and polarization distortions were computed as the fiber underwent various degrees of bending. The vector finite element method using high order Nedelec basis functions along with symplectic time integration schemes provided the numerical approximations. Thus, continuity properties of the fields across interfaces were maintained, energy was conserved in the semi-discrete sense and the detrimental effects of numerical dispersion which commonly plague electrically large problems such as these were kept to a minimum.

REFERENCES

[1] C. Vassallo, *Optical Waveguide Concepts*. Elsevier Sci. Pub., 1991.
[2] F. Wilczewski, "Bending loss of leaky modes in optical fibers with arbitrary index profiles," *Optics Lett.*, vol. 9, pp. 1031–1033, 1994.
[3] W. A. Gambling, H. Matsumura, and C. M. Ragdale, "Curvature and microbending losses in single-mode fibres," *Optical and Quantum Electronics*, vol. 11, no. 1, pp. 43–5, 1979.
[4] D. Marcuse, "Curvature loss formula for optical fibers," *J. Opt. Soc. Am.*, vol. 66, no. 3, pp. 216–220, 1976.
[5] G. Rodrigue and D. White, "A vector finite element time-domain method for solving Maxwell's equations on unstructured hexahedral grids," *SIAM J. Sci. Comp.*, vol. 23, no. 3, pp. 683–706, 2001.
[6] R. Rieben, G. Rodrigue, and D. White, "A high order mixed vector finite element method for solving the time dependent Maxwell equations on unstructured grids," *J. Comput. Phys.*, October 2004, in press.
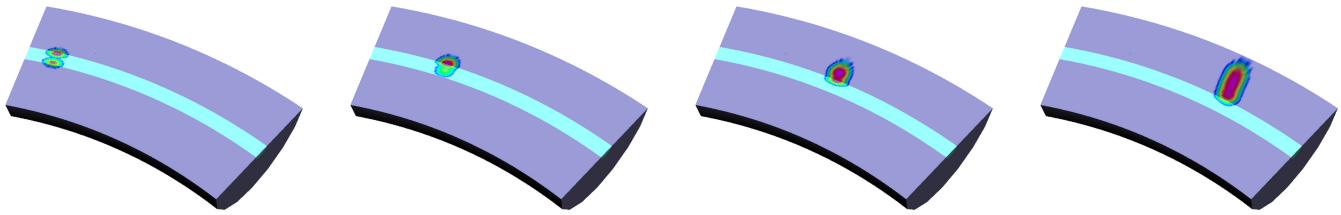
Fig. 4. Snapshots of the base 10 log of the electromagnetic energy in the 30 degree bent fiber at time $t = 0.1333ps, 0.2667ps, 4.000ps$ and $0.5333ps$.
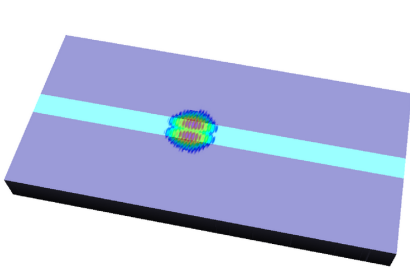

Fig. 5. Snapshot at time $t = 0.36ps$ of base 10 log of Poynting field magnitude for straight fiber.
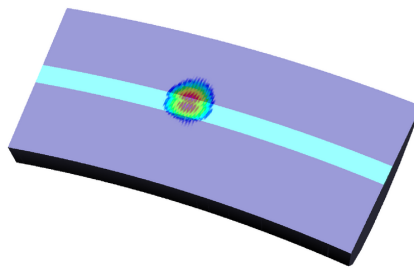
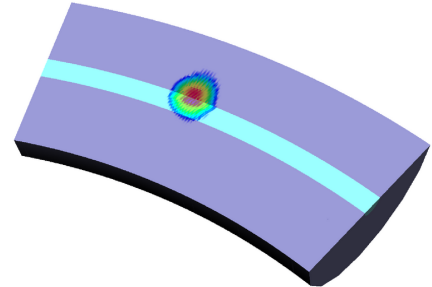Fig. 6. Snapshot at time $t = 0.36ps$ of base 10 log of Poynting field magnitude for 15 degree bent fiber.

Fig. 7. Snapshot at time $t = 0.36ps$ of base 10 log of Poynting field magnitude for 30 degree bent fiber.

[7] J. C. Nédélec, "Mixed finite elements in R3," *Numer. Math.*, vol. 35, pp. 315–341, 1980.
[8] R. Rieben, D. White, and G. Rodrigue, "Improved conditioning of finite element matrices using new high order interpolatory bases," *IEEE Trans. Ant. Prop.*, vol. 52, no. 10, pp. 2675–2683, October 2004.
[9] ——, "High order symplectic integration methods for finite element solutions to time dependent Maxwell equations," *IEEE Trans. Ant. Prop.*, vol. 52, no. 8, pp. 2190–2195, August 2004.
[10] J. Saijonmaa and D. Yevick, "Beam-propagation analysis of loss in bent optical waveguides and fibers," *J. Opt. Soc. Am.*, vol. 73, pp. 1785–1791, 1983.
[11] K.Thyagarajan, M. Shenoy, and A. Ghatak, "Accurate numerical method for the calculation of bending loss in optical waveguides using a matrix approach," *Optics Lett.*, vol. 12, pp. 296–298.
[12] D. R. Goff, *Fiber Optic Reference Guide*, 2nd ed., 1999.

Joe Koning is an engineer in the Electrical Engineering Department at Lawrence Livermore National Laboratory. Joe is a member of the Computational Engineering Group and is actively researching three-dimensional full-vectoral electrodynamics and three-dimensional multiphase fluid dynamics. Joe earned his Ph.D. in Engineering-Applied science with a computational physics emphasis from the University of California at Davis in 2004. His studies at Davis focused on three-dimensional simulations for linear wave equations using a discrete differential forms finite element formulation. Joe received a B.A. in Physics from the University of California at Berkeley in 1992 and an M.S. in Computational Physics from San Jose State University in 1997.
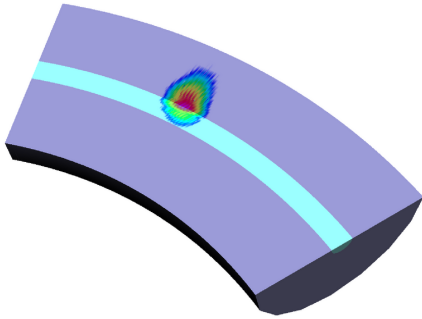
Fig. 8. Snapshot at time $t = 0.36ps$ of base 10 log of Poynting field magnitude for 45 degree bent fiber.
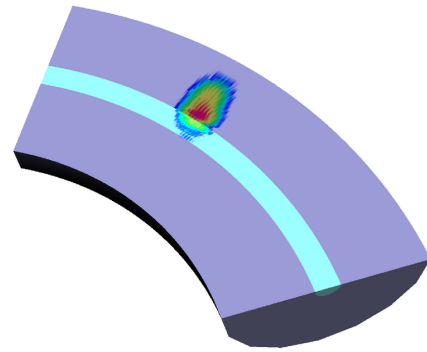

Fig. 9. Snapshot at time $t = 0.36ps$ of base 10 log of Poynting field magnitude for 60 degree bent fiber.
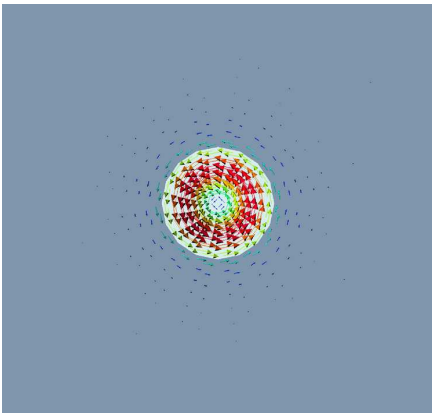

Fig. 10. Snapshot at time $t = 0.36ps$ of electric field vector for straight fiber sliced in a plane with unit normal $(0, 0, 1)$.
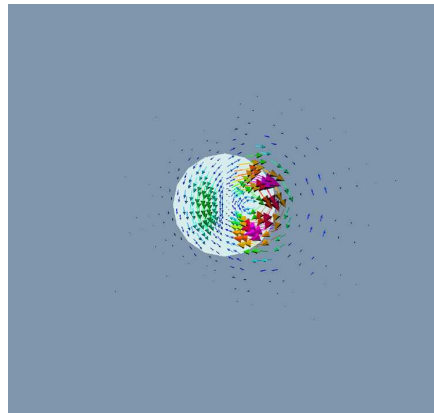

Fig. 11. Snapshot at time $t = 0.36ps$ of electric field vector for 15 degree bent fiber sliced in a plane with unit normal $(-0.111, 0, 0.994)$.
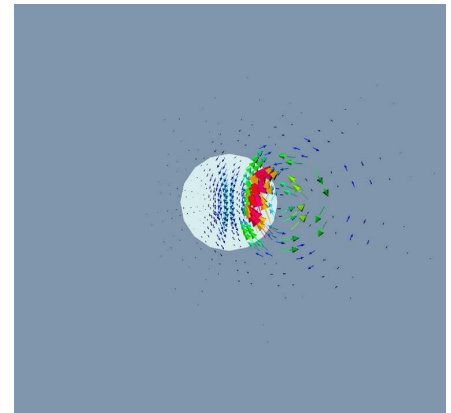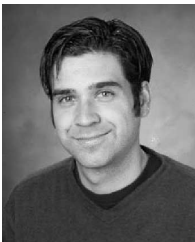

Fig. 12. Snapshot at time $t = 0.36ps$ of electric field vector for 30 degree bent fiber sliced in a plane with unit normal $(-0.221, 0, 0.975)$.

Robert N. Rieben (IEEE member) received his B.S. in physics from the University of California at Riverside in 1999 and his Ph.D. in engineering / applied science from the Department of Applied Science, University of California at Davis. He is currently a post-doctoral researcher with the Defense Sciences Engineering Division at the Lawrence Livermore National Laboratory. His research interests include massively parallel physics simulations using high order numerical methods, time-domain vector finite element methods, the modeling and simulation of electromagnetic wave propagation and photonic crystals and photonic band-gap structures.

Garry H. Rodrigue received his Ph.D. degree from the University of Southern California, Los Angeles, California for work in numerical mathematics. He is currently a Professor with the Department of Applied Science, University of California at Davis, California. He is also an adjunct member of the Institute for Scientific Computing Research at the Lawrence Livermore National Laboratory in Livermore, California. His research interests are in large scale numerical simulations of phenomenon in electromagnetics, optics, fluid dynamics and magnetohydrodynamics.
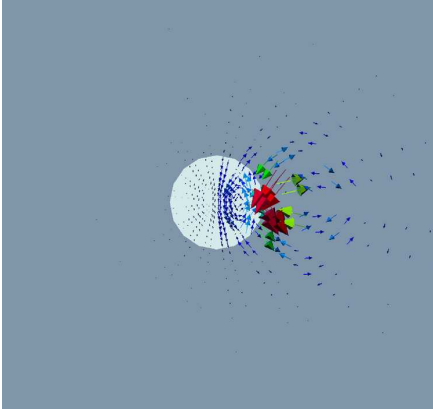
Fig. 13. Snapshot at time $t = 0.36ps$ of electric field vector for 45 degre bent fiber sliced in a plane with unit normal $(-0.328, 0, 0.945)$.
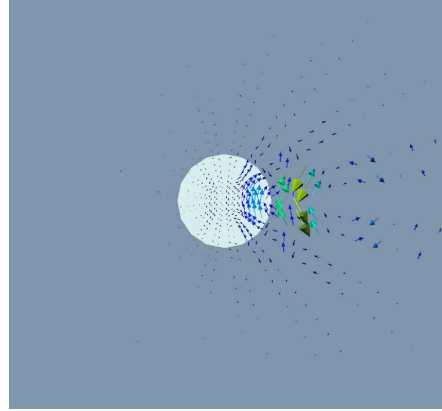

Fig. 14. Snapshot at time $t = 0.36ps$ of electric field vector for 60 degree bent fiber sliced in a plane with unit normal $(-0.431, 0, 0.902)$.